



Aeroacoustic Investigation of Refrigerator Air Duct and Flow Systems

Hazal Berfin Demir¹, Bayram Çelik², Koray Erdoğan³

¹Aeronautical and Astronautical Engineering Department, Istanbul Technical University, Istanbul, Turkey.
hazalberfindemir@gmail.com

²Astronautical Engineering Department, Istanbul Technical University, Istanbul, Turkey
celikbay@itu.edu.tr

³Vibration and Acoustics Department, Arçelik Central R&D, Istanbul, Turkey.
koray.erdogan@arcelik.com

As refrigerators become indispensable for modern kitchens, the comfort they provide to the user has become important as well as their cooling performance. One of the parameters affecting user comfort is the sound power level of the product. In No-frost refrigerators, the most dominant sound source after compressor is the fans. This paper describes the numerical and experimental aeroacoustic performance investigation of a No-frost refrigerator freezer compartment. The study consists of two main parts. The first part covers the numerical investigation of flow and flow induced noise around the axial fan in the freezer compartment. The numerical solution, including pressure based unsteady RANS and Ffowcs Williams & Hawkings solutions, is experimentally verified with the volume flow rate and sound pressure information at certain points. In the second part of the study, this validated model is applied for the entire freezer section. Regions where the flow noise is intense are determined by looking at the velocity and turbulent kinetic energy distribution. The sound pressures created by the sound waves emitted from the front, back and side surfaces of the numerically analysed freezer volume at certain microphone positions are examined. The compatibility between numerical and experimental studies was examined and suggestions were made to increase it.

Keywords: refrigerator, freezer compartment, aeroacoustic, URANS, Ffowcs Williams & Hawkings

1 Introduction

Refrigeration is a process that supplies cooling by providing heat transfer from a volume at lower temperature to higher temperature. One of the usage area of this process is refrigerators to keep nutrients fresh by decreasing the rate of spoilage. The first stones of artificial refrigeration were built by Professor William Cullen in 1755. He used diethyl ether and a pump to reduce the heat of surrounding area [1]. In 1911, an American company invented the first commercial domestic refrigerator. The refrigerator based on vapour absorption process was first made in 1931. In addition, the first dual temperature refrigerator with two chambers was introduced in 1939 [2].

With the developments in cooling technology, the use of static refrigerators in homes was increased over time. Static refrigerator models are consist of four main parts of vapour compression system which are compressor, evaporator, condenser and capillary. These refrigerator model generally include both freezer and fresh food compartments. Evaporator pipes are located on the top, bottom and side surfaces of the freezer and back surface of the fresh food compartment. Since the refrigerant is much colder than the refrigerator inside, icing occurs on the evaporator related surfaces over time. Ice layer thicker than 3-4 mm reduces the cooling performance and energy efficiency of the product. In order to overcome this problem, the ice layer should be removed with

defrosting regularly. In 1987, new No-frost technology was introduced with its several usefulness. No-frost technology comprises powerful fans additional to four main compression vapour cycle components. These fans absorb the relatively hot air in the cabinet towards the evaporator pipes. Then, cooled air from the interaction with evaporator are blew out to the cabinet inside.

Although the cooling performance has been improved with the No-frost technology, the acoustic emission has increased. Engineering studies are carried out to reduce the sound power level of the refrigerator in order to increase user comfort and comply with acoustic regulations. In No-frost refrigerators, the most dominant sound source after compressor is the fans. The types of fans used are usually axial or radial. Experimental and numerical aeroacoustic performance studies of these fan types have been studied in the literature [3-8]. This paper aims to examine aeroacoustic performance of a No-frost refrigerator and to make design recommendations to reduce acoustic emission.

2 Solo Axial Fan Investigation

The axial fan in the freezer compartment consists of 4 blades equally spaced on the hub as presented in Figure 1. The outer diameter of the fan is 115 mm and the tip chord length is 82 mm. The operating speed of the fan is 1200 rpm. Depending on the blade tip speed and tip chord length, Reynolds Number is approximately 29,500.

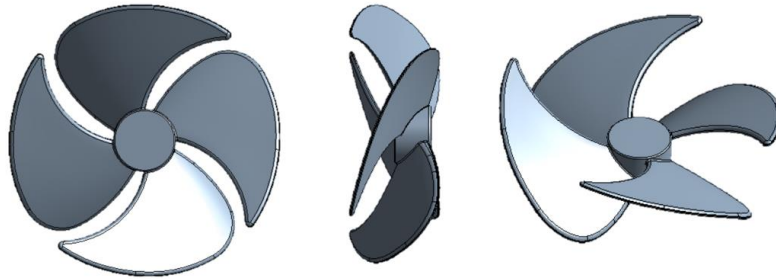


Figure 1: Freezer fan model of refrigerator

2.1 Axial Fan Numerical Investigation

In order to predict the flow characteristic properties and performance, three dimensional incompressible Unsteady Reynolds Averaged Navier Stokes (URANS) were used as the governing equations.

$$\frac{\partial \bar{v}_i}{\partial x_i} = 0 \quad (1)$$

$$\frac{\partial \bar{v}_i}{\partial t} + \frac{\partial}{\partial x_j} (\bar{v}_i \bar{v}_j) = -\frac{1}{\rho} \frac{\partial \bar{p}}{\partial x_i} + \nu \frac{\partial^2 \bar{v}_i}{\partial x_j \partial x_j} - \frac{\partial \overline{v_i'' v_j''}}{\partial x_j} \quad (2)$$

The computational fluid dynamics analysis were performed by ANSYS Fluent which is based on finite volume method. Fluent solved the flow governing equations under three dimensional, unsteady and time dependent, viscous, incompressible flow assumptions. In the analysis, Shear Stress Transport (SST) model which is combination of $k - \epsilon$ and $k - \omega$ was preferred as the turbulence model. The $k - \epsilon$ turbulent model is weak at determining shear stress in adverse pressure gradient flows and it requires modification for near wall region

[9]. The $k - \omega$ model is better than $k - \varepsilon$ to predict adverse pressure gradient flow's shear stress. However, it depends on the free stream value of specific turbulent dissipation rate [9]. SST model solves $k - \omega$ model in the boundary layer and $k - \varepsilon$ in the outer region. The combination of these two eddy viscosity models uses $\omega = \frac{\varepsilon}{(\beta^*k)}$ relation where $\beta^* = c_{\mu}$. In order to switch the coefficients from $k - \omega$ to $k - \varepsilon$, F_1 function is used. It is 1 for $k - \omega$ region and 0 for $k - \varepsilon$ region.

$$F_1 = \tanh(\xi^4) \quad (3)$$

$$\xi = \min \left[\max \left\{ \frac{\sqrt{k}}{\beta^* \omega d}, \frac{500\nu}{d^2 \omega} \right\} \frac{4\sigma_{\omega_{k-\varepsilon}} k}{CD_{\omega} d^2} \right] \quad (4)$$

$$CD_{\omega} = \max \left\{ 2\sigma_{\omega_{k-\varepsilon}} \frac{1}{\omega} \frac{\partial k}{\partial x_i} \frac{\partial \omega}{\partial x_i}, 10^{-10} \right\} \quad (5)$$

$$\nu_t = \frac{\alpha_1 k}{\max(\alpha_1 \omega, |\bar{s}| F_2)} \quad (6)$$

$$F_2 = \tanh(\eta^2) \quad (7)$$

$$\eta = \max \left\{ \frac{2k^{1/2}}{\beta^* \omega d}, \frac{500\nu}{d^2 \omega} \right\} \quad (8)$$

During the analysis, the flow area was divided into three regions, one rotating and two stationary, and the movement of these regions relative to each other was modelled by sliding mesh method. The flow volume was divided into finite volumes by using polyhedral mesh types on the walls and boundary layer; and hexahedron mesh types in the core. Mesh quality was checked according to skewness values. Mesh quantities and qualities are indicated in Table 1. As the boundary conditions, 0 pa gauge total pressure at the inlet and 0 pa atmospheric pressure (gauge) at the outlet were defined.

Table 1 – Detailed mesh information of solo axial fan fluid domain

Region name	Maximum quality	Cell count
Up fluid	0.6935	789,292
Down fluid	0.7764	444,623
Rotating body	0.8074	7,481,914
Overall summary	0.8074	8,715,829

As it is indicated in Figure 2, the axial fan produces turbulence. It starts at the wing tips, which are also the region with maximum turbulence kinetic energy. The eddies coming out of the wing tip continue along the wing line with decreasing energy.

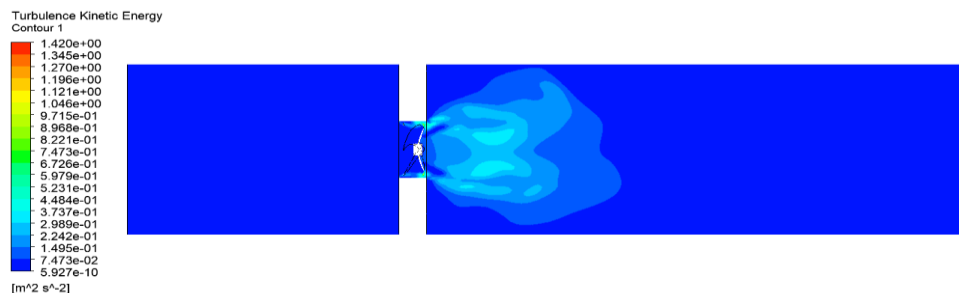


Figure 2: Turbulence kinetic energy contour plot of solo fan wind tunnel simulation

A low-energy zone is formed behind the hub. However, after a short distance, the energy of the eddies emanating from the wings affects this region as well. Energy distribution shows a symmetrical distribution when the fan center is taken as reference. At a distance of about 7 times the rotating body, the high-energy turbulence field ends.

As the second step of the numerical investigation of solo axial fan, acoustic model was established. Numerical acoustic studies have some difficulties due to the low energy of acoustic waves and the challenge on calculating the properties that are the source of sounds in the near field. These difficulties can be minimized by correct creation of the flow volume, fine mesh removal, and installation of the appropriate model. In these hybrid aeroacoustic solutions from ANSYS, the outputs of the flow analyses form the inputs for the acoustic analysis. The acoustic model used was Ffowcs Williams & Hawkings (FW-H), one of the acoustic solutions provided by ANSYS. The FW-H equation is an inhomogeneous wave equation obtained by solving the continuity equation and the Navier-Stokes equations together.

$$\frac{1}{a_0^2} \frac{\partial^2 p'}{\partial t'^2} - \nabla^2 p' = \frac{\partial^2}{\partial x_i \partial x_j} \{T_{ij} H(f)\} - \frac{\partial}{\partial x_i} \{[P_{ij} n_j + \rho u_i (u_n - v_n)] \delta(f)\} + \frac{\partial}{\partial t} \{[\rho_0 v_n + \rho (u_n - v_n)] \delta(f)\} \quad (9)$$

The first term on the right side of Equation 9 indicates quadrupole source, meaning volume distribution due to flow outside surfaces. The second term indicates a dipole source, which is a surface distribution due to the interaction of the flow with moving bodies, and the third term indicates a monopole source, which is a surface distribution due to the volume displacement of the liquid during the movement of the surfaces.

2.2 Axial Fan Experimental Investigation

Within this study, model validation was performed for both the flow solution and the acoustic solution separately. For flow solution verification, a volumetric flow rate test was performed in the wind tunnel of the respective axial fan. There are three nozzles with 0.8", 1.6" and 3" diameters in the second section of the axial wind tunnel constructed according to ANSI AMCA 210-85 standard. It is decided which nozzle to be closed and which to be left open during the measurement by looking at the characteristic curves determined for flow and pressure. The purpose of the wire plates placed one after the other in various parts of the tunnel is to ensure the uniformity of the flow and thus to prevent incorrect measurements that may arise from turbulence.

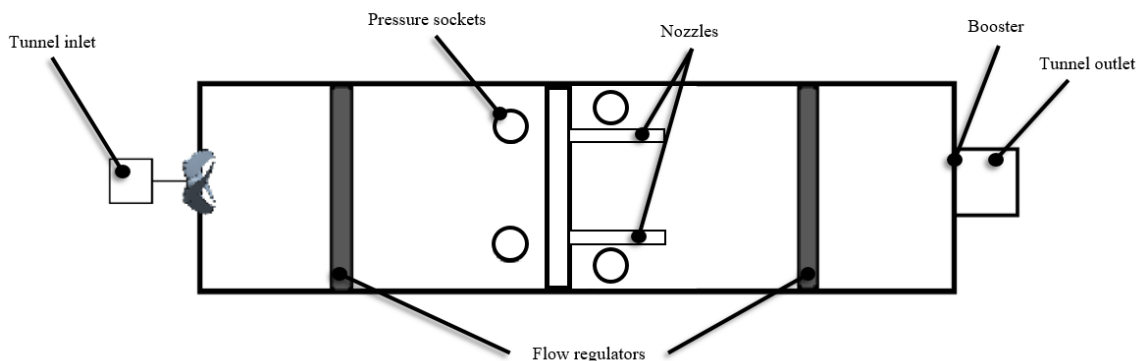


Figure 3: Wind tunnel schematic drawing

Flow measurements up to $1000 \text{ m}^3/\text{h}$ can be made in the wind tunnel. The measuring setup consists of flow regulators, nozzles, pressure sockets and the fan located at the air outlet of the wind tunnel, as shown in Figure 3. The P-V diagram of the working fan was created by measurements made in the wind tunnel whose schematic is shown. The axial fan is sealed to the tunnel by means of the duct on the blowing side. After the completion of the test preparations, the tests are carried out in room conditions, with the use of appropriate nozzles. Experiments are made in cases where the tunnel exit is fully closed and fully open and by using a booster when necessary. The measuring points are pressure sockets placed at the inlet and outlet of the nozzles in accordance with the standard. After the preparations, the axial fan was driven between 6 and 12 volts and the volume flow rate under different pressure loads was reflected in the graph shown in Figure 4. As obtained in numerical studies, the volumetric flow rate was confirmed by experiments as 19 L/s under 0 pressure difference for 1200 rpm rotation speed. These operating conditions were reached when the fan is running at 6 volts.

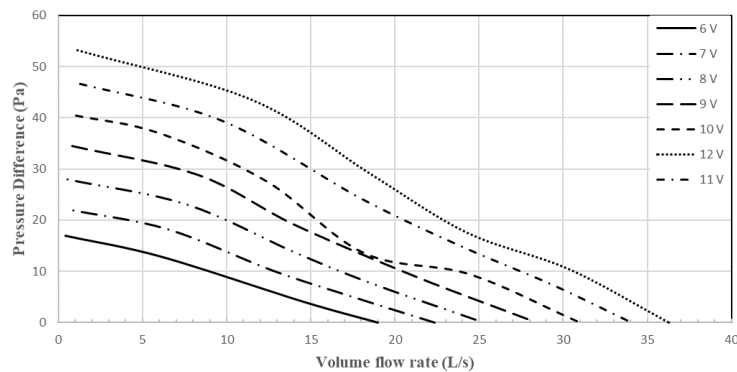


Figure 4: P-V diagram of the solo fan

Acoustic experiments were carried out in a full anechoic room with dimensions of $6.95 \text{ m} \times 6 \text{ m} \times 6 \text{ m}$. The microphones used for the measurements are B&K 4955. Sound pressure data were collected from a total of 12 points placed at equal angular distances around the fan. Comparison of the experimental measurement results from the fan blowing zone with the numerical measurement results is shown in Figure 5. Blade passing frequency (BPF) of the axial fan is 80 Hz . This distinctive frequency was also obtained in numerical studies in accordance with the experimental results. Both numerical and experimental curves have similar behavior, although the level of numerical data is lower.

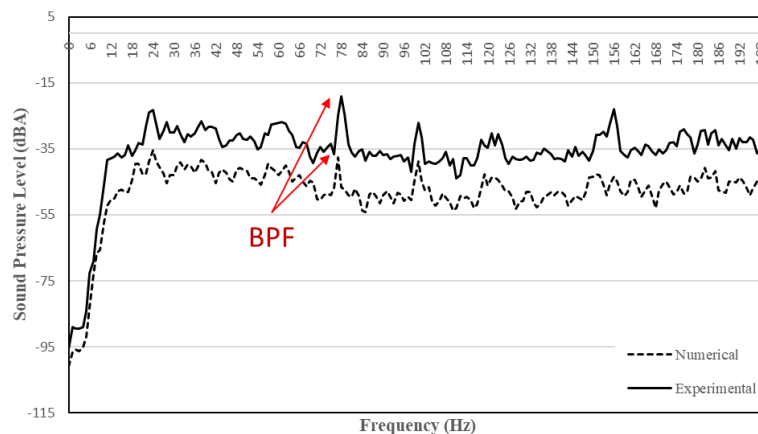


Figure 5: Sound pressure level comparison

This amplitude difference between the two curves may be due to fan motor noise and some assumptions used to speed up numerical calculations. By using more realistic flow models such as DNS and LES, the turbulence field can be resolved at a higher rate and the obtained results can be closer to the experimental results.

3 Freezer Compartment Investigation

The simplified freezer compartment geometry includes 3 drawers, an evaporator mask, an axial fan and the walls surrounding them which is shown in Figure 6. The freezer volume is recessed inward as the compressor and other cabinet bottom components are located in the rear lower compartment. The evaporator mask has parallel lines with the geometry of the back wall of the volume. The axial fan is located in the upper middle part of the mask. The drawers are placed in such a way that there is enough space between the evaporator mask and the drawers to ensure air flow.

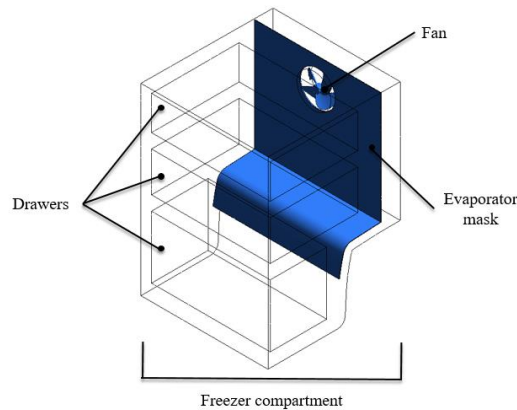


Figure 6: Freezer compartment model

3.1 Freezer Numerical Investigation

For flow analyses of the freezer volume, transient SST $k - \omega$ model was used, which was previously validated with axial fan operation. The governing equations were solved under three dimensional, unsteady and time dependent, viscous, incompressible flow assumptions. The fluid domain was divided into 18,155,765 polyhedral and hexahedron meshes with the worst quality 0.83 skewness. In order to shorten the convergence time, the model was first solved steady, and after convergence, the transient was solved for 5 full rotations of the fan. Figure 7 shows turbulence kinetic energy contour plot, velocity contour plot and velocity vector plot of the freezer flow analysis, respectively.

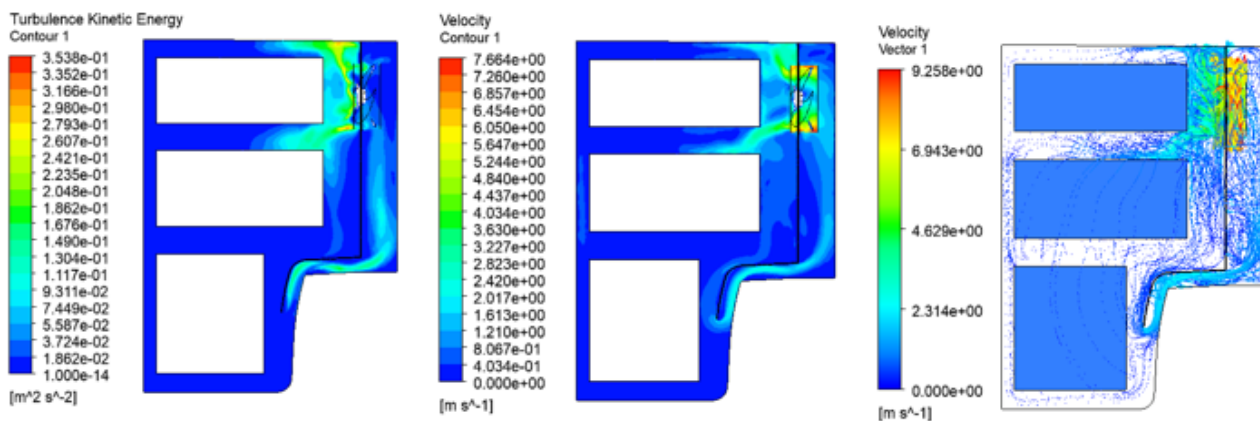


Figure 7: Plots of freezer compartment flow features

The fan draws air from the lower part of the evaporator mask and blows it towards the upper drawer. Turbulence formation starts at the wing tips as observed in solo fan analyses. The eddies coming out of the fan blade tips concentrate especially on the upper wall of the freezer volume and in the space between the upper two drawers. Besides, turbulence is observed in the region starting from the lower part of the evaporator mask and extending towards the fan suction area.

After the flow solution, which takes 5 fan revolutions, acoustic analysis was performed for the time required for the fan to make one full rotation. As the acoustic solution model, FW-H was used.

3.2 Freezer Experimental Investigation

In this part of the study, acoustic experiments were carried. Experiments were made in a Full Anechoic Room where solo fan analyses were also performed. The experimental environment is shown in Figure 8. Before starting the experiment, the fan was run for a while and expected to be in regime. Sound pressure measurements were taken from two different distances from the front, back and side surfaces of the freezer volume with B&K 4955 microphones. In order to minimize the measurement instability, the experiment was repeated at different times and averaged.



Figure 8: Acoustic test environment

Measured sound pressure level for different surfaces and distances are indicated in Table 2. Sound pressure values were measured as 26.7 at distance a and 23.3 at a distance of $2a$, in the measurements taken from the back surface. Back surface is the closest surface to the axial fan, which is the only sound source in the study. The energy of the sound waves decreases until they reach the front surface, therefore, in the measurements taken from the front surface, the sound pressure values are measured as 20.5 with a decrease of 6.2 dBA at distance a .

Table 2 – Freezer sound pressure levels

Measurement surface	Microphone distance	Sound pressure level (dBA)
Front	a	20.5
Front	$2a$	19
Back	a	26.7
Back	$2a$	23.3
Left	a	17.5
Left	$2a$	14.1
Right	a	16.5
Right	$2a$	14

Sound pressure level spectrum obtained through experiments are shown in Figure 9. BPF is clearly seen as 80, however unlike solo fan measurements, the amplitudes of the BPF harmonics are not significant.

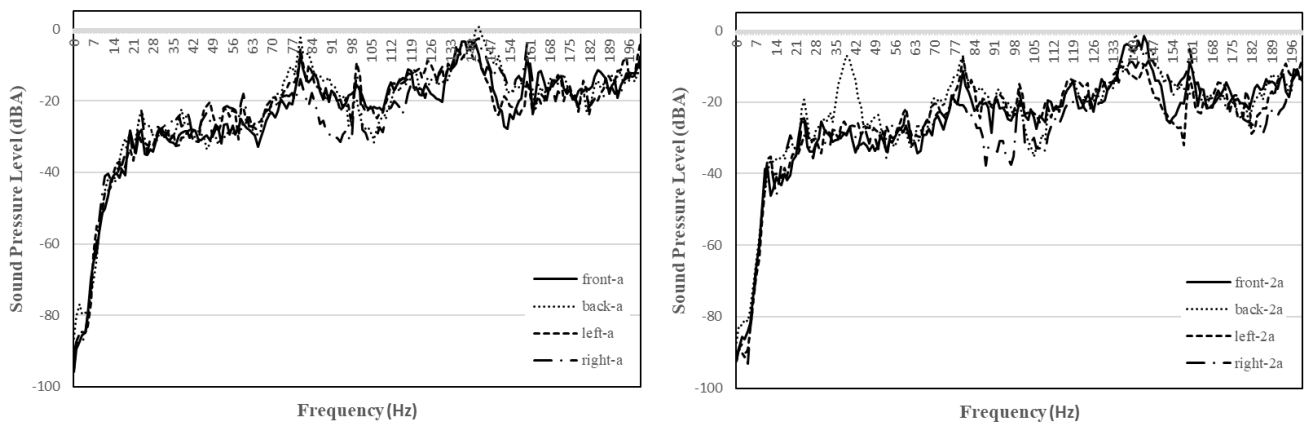


Figure 9: Sound pressure level spectrum at distance a (left) and distance $2a$ (right)

4 Conclusion

The air flow-induced noise level of the freezer volume of the combi type refrigerator was investigated. The axial fan, which is the sound source in the system, was analyzed solo and within the freezer volume. In the first step, the flow solutions of the system were modeled with unsteady RANS, SST $k - \omega$ turbulence model. The results of the flow solution were given as input to the acoustic solution with Ffowcs Williams & Hawking model. A strong agreement was observed between the results of the solo fan analysis and the experimental flow and acoustic measurements. The validated model was repeated over the entire freezer volume. By examining the turbulence formed, the parts where the flow energy increased were determined. In addition to being intense especially at the axial fan blade tips, turbulence was also observed in the upper ceiling, between the upper two drawers and behind the evaporator mask. Sound pressure data were collected from the front, back and side surfaces within the scope of the freezer volume experimental acoustic studies. It has been observed that the pressure values created by the sound waves emitted from the back surface, which is the closest surface to the sound source, at the microphone positions are the highest. Since the axial fan cannot be changed, acoustic improvement can be achieved with various geometric optimizations and air duct designs by focusing on the turbulence formation behind the evaporator mask.

5 References

- [1] Arora, R. C. Refrigeration and air conditioning, New Delhi (India), 2010.
- [2] Dixit, U. S.; Hazarika, M.; Davim J. P. *A brief history of mechanical engineering*, Springer, Switzerland, Edition 1, 2017.
- [3] Zhao, X.; Sun, J.; Zhang, Z. Prediction and measurement of axial flow fan aerodynamic and aeroacoustic performance in a split-type-air-conditioner outdoor unit, *International Journal of Refrigeration*, Volume 36, 2013, Pages 1098-1108.

- [4] Jiang, C.; Chen, J.; Chen, Z.; Tian, J.; OuYang, H.; Du Z. Experimental and numerical study on aeroacoustic sound of axial flow fan in room air conditioner, *Applied Acoustics*, Volume 68, 2007, Pages 458-472.
- [5] Heo, S.; Cheong, C.; Kim T. Development of low-noise centrifugal fans for a refrigerator using inclined S-shaped trailing edge, *International Journal of Refrigeration*, Volume 34, 2011, Pages 20176-2091.
- [6] Bruccieri, B. M.; Richards, C. M. Application of the aeroacoustic analogy to a shrouded, subsonic, radial fan, *Journal of Sound and Vibration*, Volume 385, Pages 125-137.
- [7] Sturm, M.; Sanjose, M.; Moreau, S.; Carolus, T. *Aeroacoustic simulation of an axial fan including the full test rig by using the Lattice Boltzmann method*, Fan 2015, Lyon (France).
- [8] Hu, B.; OuYang H.; Wu, Y.; Jin G.; Qiang, X.; Du, Z.; Numerical prediction of the interaction noise radiated from an axial fan, *Applied Acoustics*, Volume 74, Pages 544-552.
- [9] Davidson, L.; *Fluid mechanics, turbulent flow and turbulence modelling*, Göteborg (Sweden), 2019.